JOURNAL OF AIRCRAFT
Vol. 32, No. 3, May–June 1995

Flow Physics of Critical States for Rolling Delta Wings

Lars E. Ericsson*
Mountain View, California 94040

A delta wing rolling at high flow inclination has two well-documented critical states. One occurs when the breakdown of the leeside leading-edge vortex passes over the trailing edge, and the other when the breakdown of the windward vortex reaches the apex. The flow physics associated with those critical states are described for a sharp-edged 65-deg delta wing rolling around an axis inclined 30 deg to the freestream. It is shown how the measured, extremely nonlinear, unsteady aerodynamics result from the roll-rate-induced camber effect in conjunction with convective flow time lag effects.

Nomenclature

b = wingspan
c = wing root chord
f = oscillation frequency
k = reduced frequency, $\omega b/2U_\infty$
l = rolling moment: coefficient, $C_l = l/(\rho_\infty U_\infty^2/2)Sb$
l' = sectional lift: coefficient, $c_l = l'/(\rho_\infty U_\infty^2/2)c$
M = Mach number
$P(t)$ = phase plane characteristics, $\phi(t)$, $\dot{\phi}(t)$
p = aerodynamic pressure: coefficient, $C_p = (p - p_\infty)/(\rho_\infty U_\infty^2/2)$
S = reference area, projected wing area
s = local semispan
t = time
U = horizontal velocity
x = axial body-fixed coordinate
y = spanwise body-fixed coordinate
α = angle of attack
Δ = increment or amplitude
Δt = time lag
$\Delta\phi$ = roll oscillation amplitude
η = dimensionless y coordinate, y/s
θ_c = cone half-angle, Fig. 6
Λ = leading-edge sweep angle
ξ = dimensionless x coordinate, x/c
ρ = air density
σ = inclination of body axis, 30 deg
ϕ = roll angle
$\dot{\phi}$ = reduced roll rate, $\dot{\phi}b/2U_\infty$
$\phi(0)$ = initial roll angle
ϕ_0 = mean roll angle
ω = angular frequency, $2\pi f$

Subscripts
B = vortex breakdown
max = maximum
s = separation
W = wing
∞ = freestream conditions

Differential symbol
$\dot{\phi}$ = $\partial\phi/\partial t$

Presented as Paper 93-3683 at the AIAA Atmospheric Flight Mechanics Conference, Monterey, CA, Aug. 9–13, 1993; received Dec. 7, 1993; revision received Oct. 21, 1994; accepted for publication Oct. 31, 1994.

*Consulting Engineer. Fellow AIAA.

Introduction

THE unsteady aerodynamics of a sharp-edged 65-deg delta wing, describing high-rate, large-amplitude roll oscillations around the body axis at 30-deg flow inclination, have been shown to be surprisingly complex.[1,2] It was recently demonstrated that the source of the complex, highly nonlinear vehicle dynamics is the presence of critical flow states.[3] While the analysis in Ref. 3 is important for further development of nonlinear mathematical analysis, it does not tell the vehicle designer how to eliminate or minimize the adverse effects on the vehicle dynamics associated with the critical states. This requires an understanding of the flow physics behind the large nonlinear effects. This article offers a description of these flow physics, expanding on the roll-rate-induced camber effect described in Refs. 4 and 5.

The two free-to-roll time histories in Fig. 1, plotted in the phase plane, are described as follows in Ref. 3:

> Note that the trajectory for the −66° release angle (solid curve) finds the stable equilibrium point at about 0° roll, while the 57° release trims at about 21°. Both trajectories pass quite close to attractors (21° and 0° respectively) with very low rates but do not trim there.—Persistent motion history effects, perhaps related to vortex breakdown dynamics, that require more than a knowledge of the instantaneous roll angle and roll rate are a strong possibility.

The present author, who is in full agreement with this conclusion, wishes to add a description of the flow physics to the mathematical treatment presented in Ref. 3.

Discussion

Figure 2 displays the equilibrium vortex breakdown position observed at σ = 30 deg on the left, port-side half of the 65-deg delta wing.[6] The solid line is the least-square-error fit to the circular data points. The triangular data point at ϕ = 5 deg departs from this linear fit. This is in accordance with the experimental results[7] shown in Fig. 3a. When accounting for the beveled leading edge,[8] the effective alpha is less than 30 deg. For such an α value Fig. 3a indicates that the vortex breakdown would rapidly move downstream of the trailing edge if the leading-edge sweep were increased from Λ = 65 deg to a value close to Λ = 70 deg, e.g., Λ = 69 deg, the value used in Fig. 3b. Figure 3b indicates that such a change of the sweep angle occurs on the left, leeward half of the 65-deg delta wing when the roll angle exceeds ϕ = 7 deg. This is also the critical ϕ value indicated by the linear fit in Fig. 2. This critical value was used in Refs. 4 and 5 to construct the idealized $C_l(\phi)$ characteristics, shown by the solid line in Fig. 4. According to the analysis in Ref. 9 the experimental

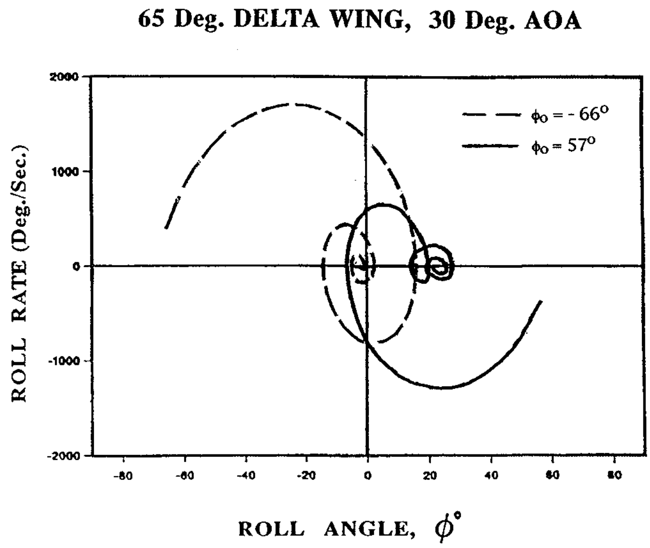

Fig. 1 Phase plane characteristics of free-to-roll motions.[3]

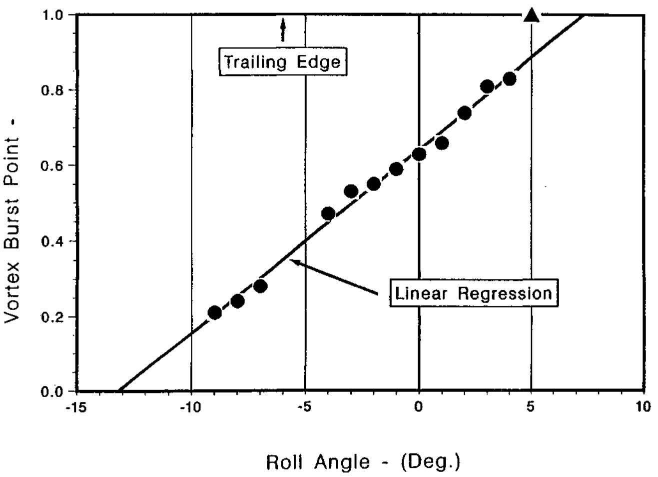

Fig. 2 Vortex breakdown position.[3]

results obtained by Wentz and Kohlman,[7] on which Fig. 3a is based, "may be untypical." This is illustrated by the compilation of experimental results for a 70-deg delta wing[10] (Fig. 5). Consequently, the experimental data[7] in Fig. 3a for Λ = 70 deg have been faired to reflect the overall data trend in Fig. 5. In Fig. 3a the independent variable is α, whereas in Fig. 3b it is the roll angle ϕ through its change of the effective leading-edge sweep of the 65-deg delta wing.

In view of the experimental results in Fig. 5, how can the idealized characteristics in Fig. 4 be justified? Considering the effect on vortex breakdown of the adverse pressure gradient at the trailing edge, one expects a change in flow-separation topology similar in some respects to that observed on a cone-cylinder at high subsonic speeds[11-14] (Fig. 6). In this case a terminal shock causes boundary-layer separation downstream of the cone-cylinder shoulder as long as $\alpha < \alpha_{crit}$, where α_{crit} < 4 deg for θ_c = 20 deg. However, when α_{crit} is exceeded, the leeside flow separation changes from this local, shock-induced type to a global type separation starting at the cone-cylinder shoulder. The flow physics behind this change in flow-separation topology is discussed at length in Ref. 11. Figure 6 shows the resulting discontinuous change of the aerodynamic loading. The sudden change of flow topology in Fig. 6 is caused by the increasing adversity of the leeside, ambient pressure gradient as the cone-cylinder shoulder is approached. Similarly, a sudden change of the vortex breakdown characteristics could be expected to occur when the trailing edge of the delta wing is approached. For the laminar flow conditions in Fig. 6 the separation topology was found to oscillate between the local and global type in the static test.[14] One can see a certain similarity between this case and the present one, where the passage of vortex breakdown over the trailing edge is associated with both motion-induced unsteadiness and static hysteresis[15] (Fig. 7). Because the static data are simply the time-averaged results of the unsteady movement of vortex breakdown, one could expect that for the rolling delta wing the $C_l(\phi)$ characteristics may fall somewhere between the idealized ones in Fig. 4 and the time-averaged ones observed in the static experiment.[1]

On the windward wing-half (in the lateral sense) the vortex breakdown moves steadily forward toward the apex with increasing roll angle. It reaches the apex for $|\phi| \approx$ 13 deg, according to the data in Fig. 2. Figure 3b indicates that the

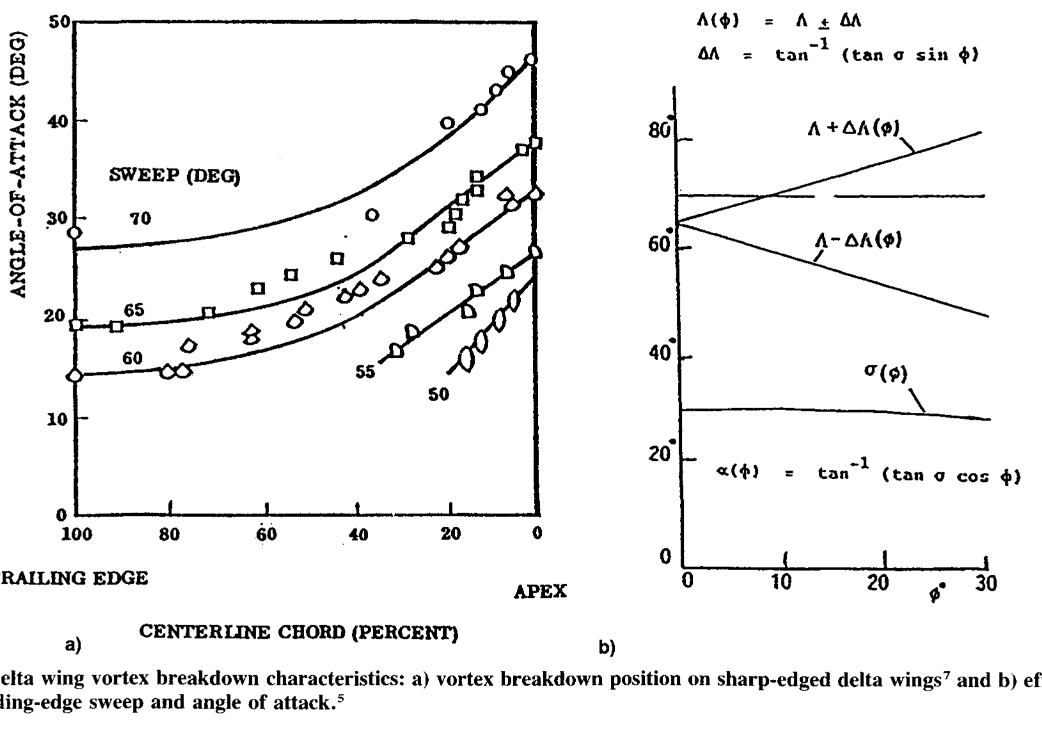

Fig. 3 Static delta wing vortex breakdown characteristics: a) vortex breakdown position on sharp-edged delta wings[7] and b) effect of roll angle on effective leading-edge sweep and angle of attack.[5]

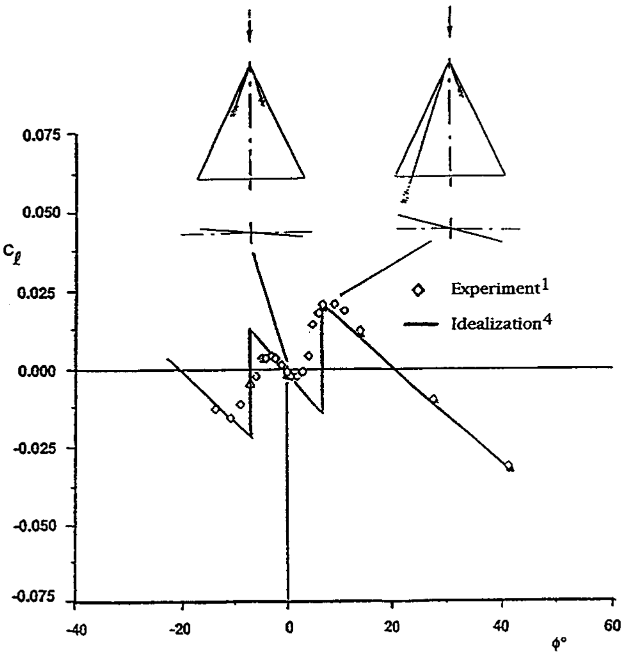

Fig. 4 Rolling moment characteristics at σ = 30 deg.[5]

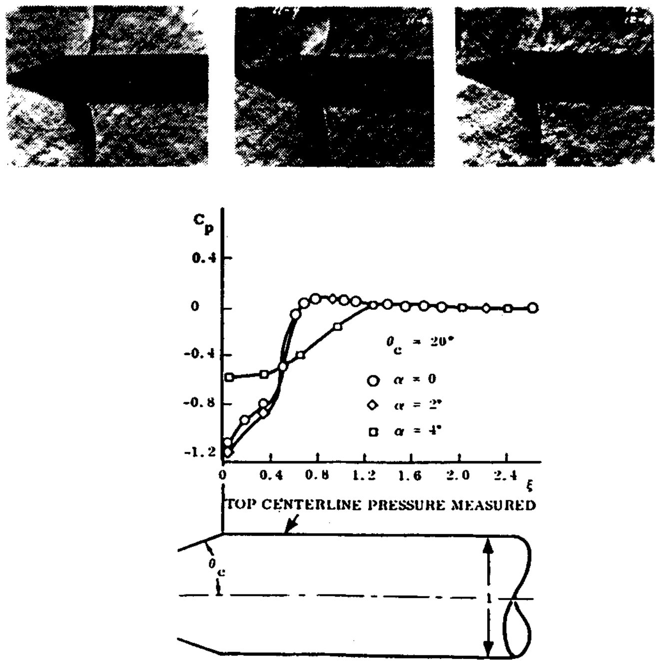

Fig. 6 Aerodynamic characteristics at M = 0.89 of a cone-cylinder body with separated flow.

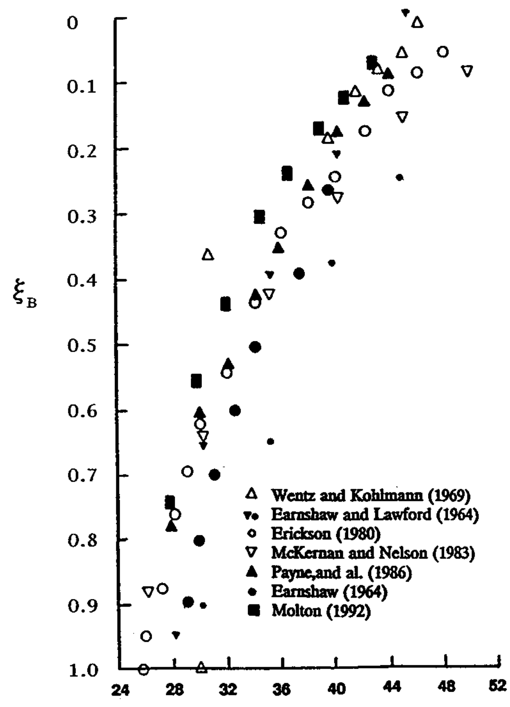

Fig. 5 Evolution with incidence of the location of breakdown over a 70-deg delta wing.[10]

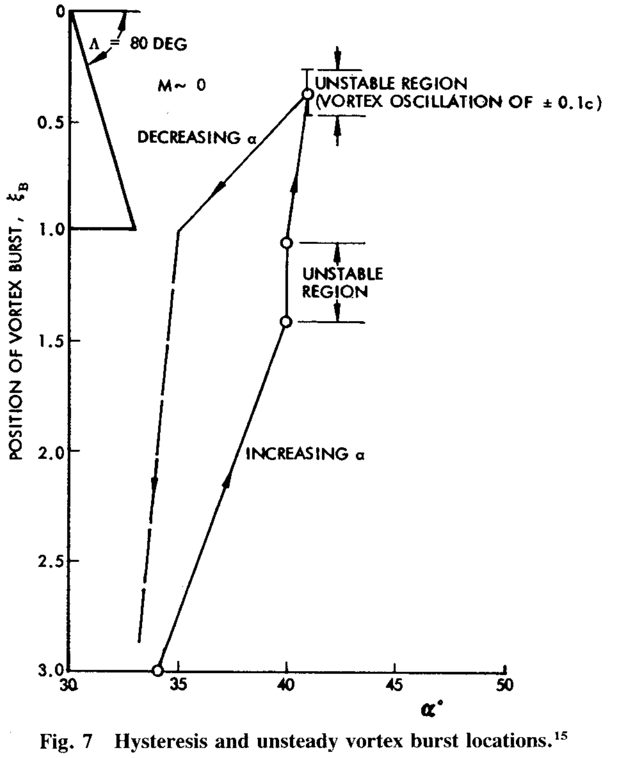

Fig. 7 Hysteresis and unsteady vortex burst locations.[15]

corresponding effective leading-edge sweep is $\Lambda \approx 58$ deg, a value consistent with the experimental results in Fig. 3a. What is critical in regard to this ϕ value for the windward wing half? When the critical ϕ value for the leeward wing half is exceeded, the steady, continuous aft movement of the vortex breakdown changed to a very rapid movement towards the trailing edge.[4,5] Recent experimental results for a 60-deg delta-wing-body configuration have revealed that an equally dramatic change of the vortex-induced loads would occur when the breakdown of the windward vortex reaches the apex[16] (Fig. 8). The suction generated by the leading-edge vortex downstream of a spiral type of vortex breakdown is wiped out (α = 39.1 deg in Fig. 8). To quote the authors of Ref. 16: "For α = 39.1° the pressure distribution on the upper surface of the wing becomes more or less constant in spanwise and chordwise direction." That is, the "spiral leading-edge vortex" is spilled downstream much as the leading-edge vortex in the case of dynamic airfoil stall.[17] Note that at $|\phi| \approx 13$ deg, where the critical state is encountered for the 65-deg delta wing (Figs. 2 and 4), the wing is at an effective angle of sideslip for which the breakdown on the leeward wing half is downstream of the trailing edge. Consequently, the breakdown formation process at the apex on the windward, dipping wing half is not affected by the breakdown process on the

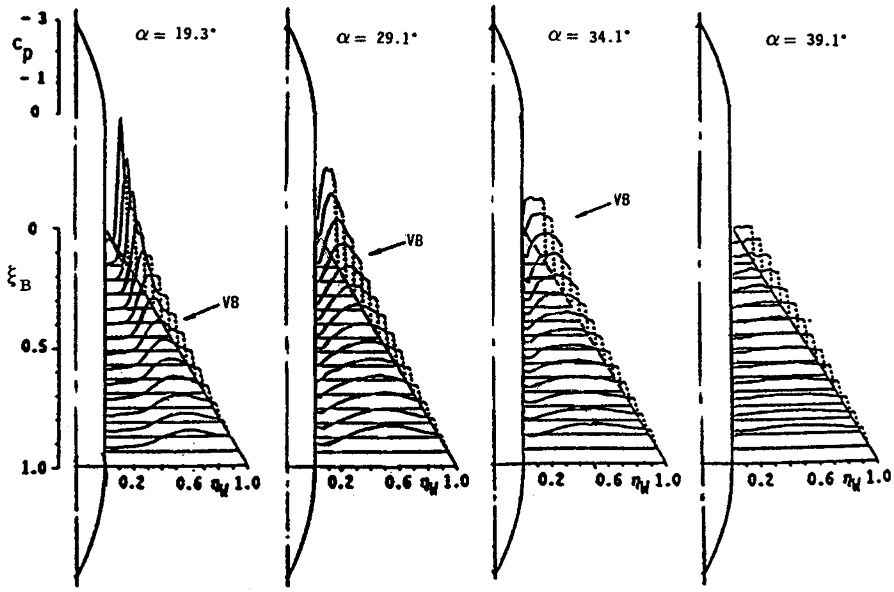

Fig. 8 Suction side pressure distribution on 60-deg delta-wing-body model at $Re = 1.4 \times 10^6$.[16]

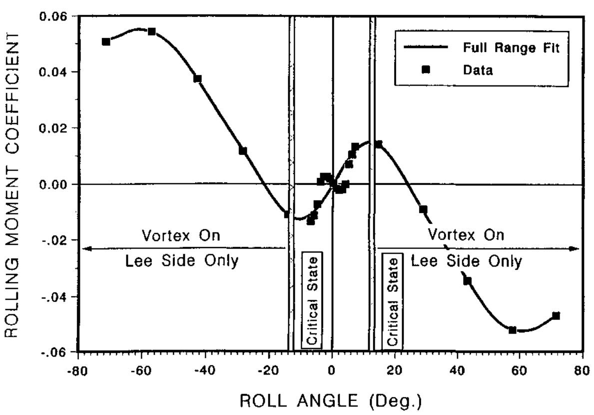

Fig. 9 Static rolling moment characteristics and critical states.[3]

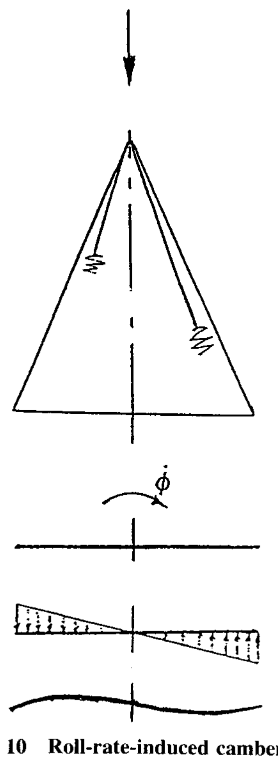

Fig. 10 Roll-rate-induced camber.[5]

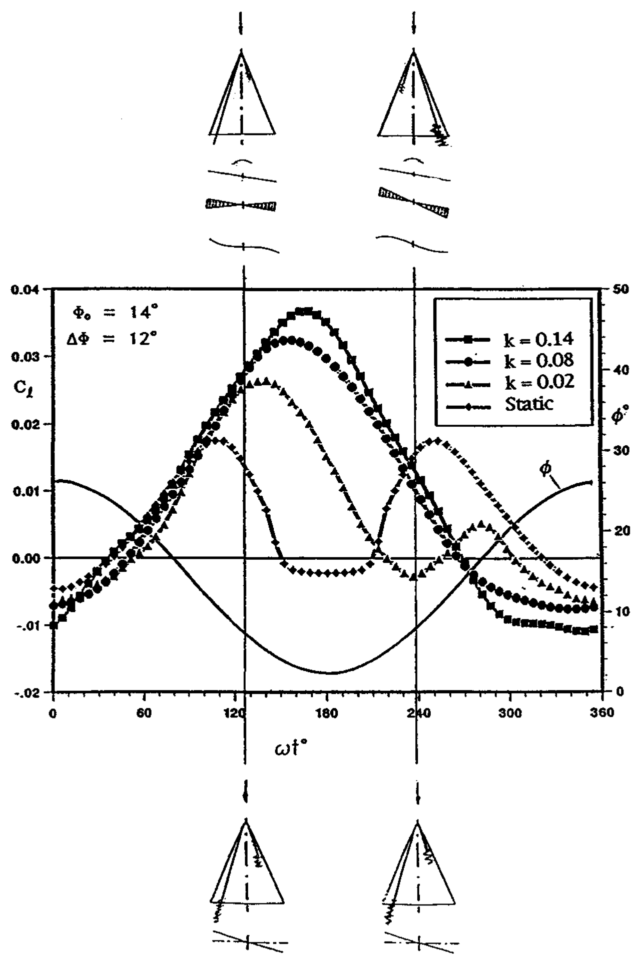

Fig. 11 Dynamic rolling moment data for $\phi_0 = 14$ deg and $\Delta\phi = 12$ deg (Ref. 3).

opposite wing half, contrary to what would be the case for symmetric flow conditions. Thus, the results in Fig. 8 for the delta-wing-body configuration illustrate what happens at the apex on the windward wing half in Fig. 4.

The static $C_l(\phi)$ characteristics of the 65-deg delta wing change in a highly nonlinear fashion in the ϕ regions containing these critical states[3] (5 deg $< |\phi| <$ 8 deg and 10 deg

< $|\phi|$ < 15 deg in Fig. 9). As discussed in Refs. 4 and 5, one can expect the roll-rate-induced camber to have especially dramatic effects in these critical ϕ regions. Figure 10 illustrates how the roll-rate-induced camber delays the breakdown of the leading-edge vortex on the downstroking wing half, whereas it promotes breakdown on the opposite, upstroking half, as has been described before[4,5] and demonstrated experimentally.[18] The dramatic effects of roll rate occur when they influence the downstream travel of breakdown towards and past the trailing edge on the leeward wing half (in the lateral sense) or the upstream travel to the apex on the windward wing half. Thus, the large effect of roll rate on the $C_l(\phi)$ characteristics observed experimentally[3] (Fig. 11) is no surprise. The role played by the roll-rate-induced camber (Fig. 10) in causing this large deviation from the static characteristics will be described in what follows.

Roll-Rate-Induced Camber Effects

At ωt = 100 deg, where $\phi \approx 12$ deg (Fig. 11), the vortex breakdown occurs behind the trailing edge on the left wing half, both in the static and dynamic case, whereas on the opposite, windward side it is about to be locked to the apex. Thus, vortex breakdown has no influence on the steady and unsteady aerodynamics. Consequently, there is no dramatic difference between static and dynamic $C_l(\phi)$ characteristics. At ωt = 126 deg, where ϕ = 7 deg, vortex breakdown is starting to occur on the left, leeward wing half in the static case. However, in the dynamic case the roll-rate-induced camber delays vortex breakdown, possibly keeping it aft of the trailing edge on the leeward wing half,[4,5] thereby generating a positive increment above the static rolling moment. Also contributing to this overshoot of the static $C_l(\phi)$ is the effect of the roll-rate-induced camber on the right, windward side, where it causes the breakdown to be closer to the apex than in the static case. The effect of the roll-rate-induced camber on leeward and windward side leading-edge vortices is illustrated by the sketches in Fig. 11 for the static (undeformed) and dynamic (instantaneously deformed) delta wings. This results in a positive rolling moment that exceeds the static $C_l(\phi)$, the more the higher the roll rate is.

When passing ωt = 180 deg, the instantaneous, quasi-steady, roll-rate-induced camber effect changes sign. At ωt = 234 deg, where ϕ = 7 deg, the vortex breakdown is in the process of passing downstream over the trailing edge of the left, leeward wing half in the static case. However, in the dynamic case the roll-rate-induced camber effect causes breakdown to occur well upstream of the trailing edge. This is illustrated by the inset sketches in Fig. 11. And on the right, windward wing half, where vortex breakdown occurs well upstream of the trailing edge in the static case, the rate-induced camber effect causes it to occur closer to the trailing edge in the dynamic case. Thus, the instantaneous dynamic effect is in this case to generate a negative rolling moment contribution, causing an "undershoot" of the static characteristics.

In comparing the two cases, ωt = 126 deg and ωt = 234 deg, one finds that in the former case the overshoot of the static $C_l(\phi)$ characteristics increases with increasing roll rate, whereas this data trend is reversed in regard to the undershoot of the static characteristics at ωt = 234 deg. The reason for this reversal is the effect of time lag on the roll-rate-induced camber, which has been neglected in the discussion so far.

Combined Effect of Dynamic Camber and Time Lag

At ωt = 180 deg, where ϕ = 2 deg and $\dot{\phi}$ = 0 in Fig. 11, the instantaneous roll-rate-induced camber is zero. The deviation between dynamic and static characteristics is generated solely by convective flow time lag effects. The effect of the roll rate on the $C_l(\phi)$ characteristics at $\dot{\phi}$ = 0 (Fig. 12a) is the residual camber effect due to time lag, as was discussed in Ref. 5 and is illustrated in Fig. 12b. In addition, one has to consider that the spilling of the spiral leading-edge vortex on the windward wing half is associated with considerable convective time lag effects, similar to those discussed in detail in Ref. 17 for dynamic airfoil stall. However, when going from ωt = 126 deg to ωt = 234 deg in Fig. 11, only the critical state at $\phi \approx 7$ deg is encountered. The effect of the time lag Δt on $|\dot{\phi}|$, and thereby on the roll-rate-induced camber, is illustrated in Fig. 13. At ωt = 126 deg, Fig. 11 shows that ϕ and $|\dot{\phi}|$ are decreasing. The corre-

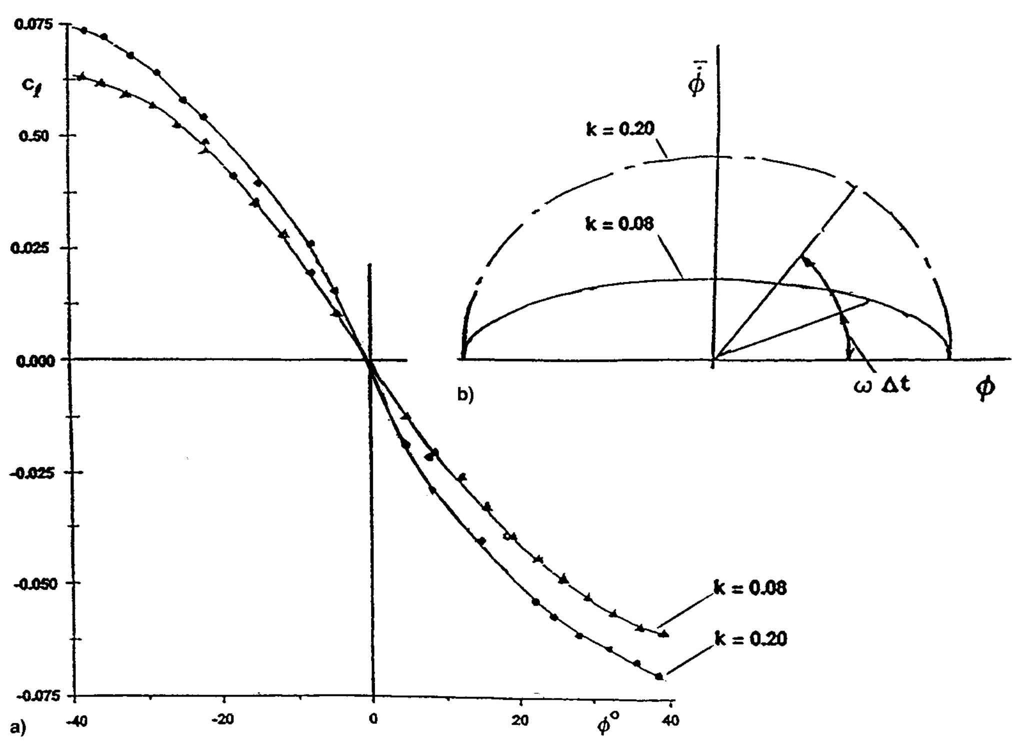

Fig. 12 Effect of roll rate on measured rolling moment at ϕ_0 = 0 and $\dot{\phi}$ = 0 (Ref. 5): a) $C_l(\phi)$ at ϕ_0 = 0 and $\dot{\phi}$ = 0 for two reduced frequencies and b) effect of time lag on residual roll-rate effect.

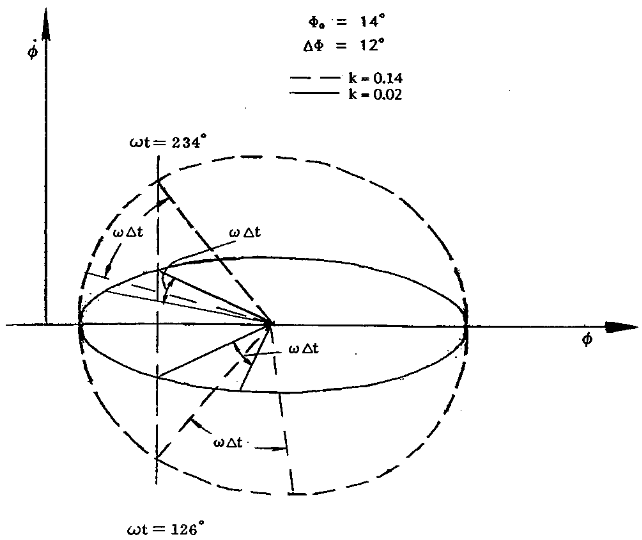

Fig. 13 Phase plane characteristics for ϕ_0 = 14 deg and $\Delta\phi$ = 12 deg.

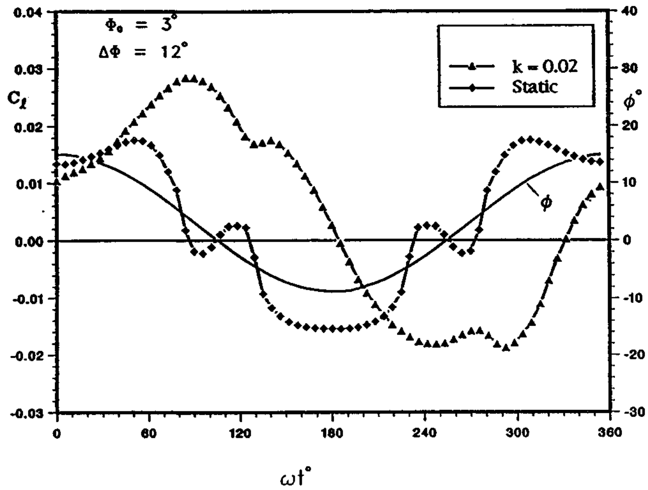

Fig. 15 Dynamic and static rolling moment data for ϕ_0 = 3 deg and $\Delta\phi$ = 12 deg (Ref. 3).

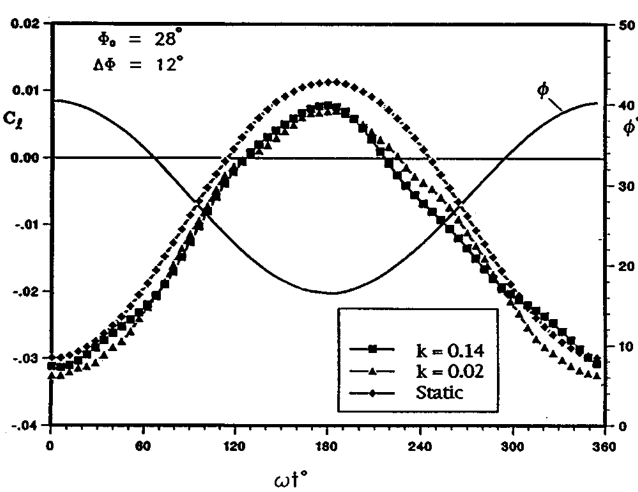

Fig. 14 Dynamic and static rolling moment data for ϕ_0 = 28 deg and $\Delta\phi$ = 12 deg (Ref. 3).

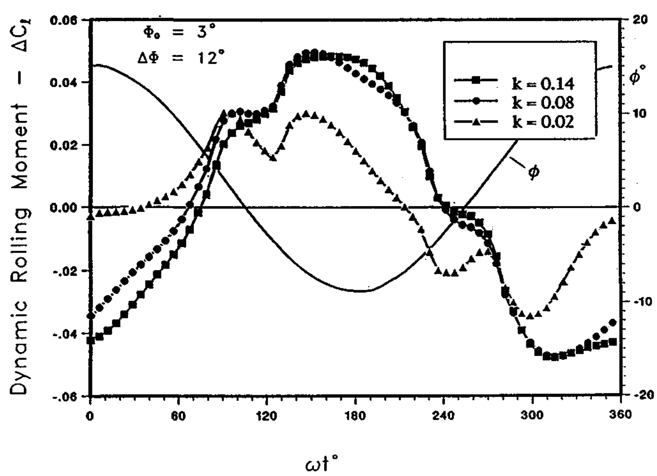

Fig. 16 Dynamic rolling moment data for ϕ_0 = 3 deg and $\Delta\phi$ = 12 deg (Ref. 3).

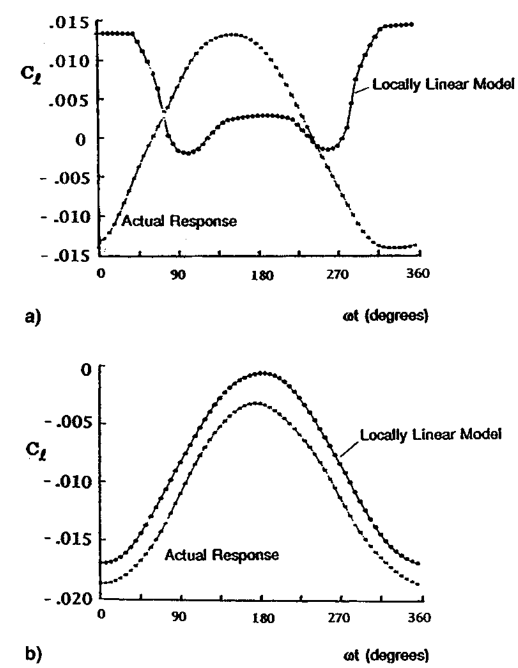

Fig. 17 Comparison between locally linear mathematical model and actual response.[3] a) ϕ_0 = 3 and b) 28 deg.

sponding phase-plane simulation is illustrated in Fig. 13 for a constant time lag Δt. It can be seen that the time lag has a very small effect, i.e., the instantaneous roll rate $|\dot{\phi}|$ is mainly determined by the magnitude of the roll rate, $|\dot{\phi}| = k\Delta\phi$. At ωt = 234 deg, Fig. 11 shows ϕ and $|\dot{\phi}|$ to increase. The corresponding phase-plane data in Fig. 13 show that in this case the effect of the time lag Δt is large, almost completely overpowering the effect of the instantaneous roll rate. This explains the different effects of frequency in Fig. 11 for ωt = 126 deg and ωt = 234 deg. Note again that the dynamic sketches in Fig. 11 illustrate the instantaneous dynamic camber, not accounting for the effect of the time lag Δt. As the roll rate is decreased, the roll-rate-induced camber effect becomes smaller. This results in less and less distortion of the static data. Thus, the experimental results for k = 0.02 in Fig. 11 tend to follow the static data trend, whereas the high frequency data deviate completely because of the large roll-rate-induced camber effect.

The results[3] in Fig. 14 demonstrate that when $\phi \geq 16$ deg, and no critical states are encountered, the dynamic data trend follows closely the static one. The reason is, of course, that the roll-rate-induced camber effect is much more benign in this case. This contrasts sharply with the results[3] in Fig. 15, where the two critical states are both encountered during portions of the oscillation cycle. For the leeward wing half

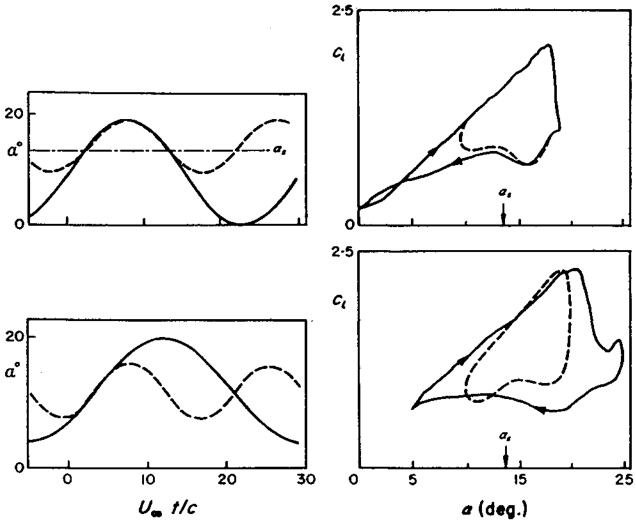

Fig. 18 Dynamic stall characteristics of the SC-1095 airfoil.[20]

the critical state at $\phi \approx 7$ deg is reached at $\omega t \approx 75$ deg, where the roll rate $|\dot{\phi}|$ is 96% of the maximum. Thus, even for the low reduced frequency $k = 0.02$ the roll-rate-induced camber effect is large. Figure 16 shows how the experimentally observed[3] data distortion due to the roll-rate-induced camber effect increases with increasing frequency. Figure 17 demonstrates that local linearization methods fail when critical states are encountered during the oscillation cycle.[3]

Phase Plane Characteristics

With the understanding gained of the flow physics the phase plane characteristics shown in Fig. 1 will be examined in more detail. That the $\phi(0) = -66$-deg release trimmed at $\phi \neq 0$ is the likely result of support interference.[19] Of more interest is the intersection at $\phi \approx -5$ deg of the two releases. According to Fig. 2 this is very close to a critical point. Thus, in the present case of the rolling delta wing it was not sufficient to simulate ϕ and $\dot{\phi}$ at the critical state. This is contrary to what has been found in the case of dynamic stall[17,20] (Fig. 18), where it is sufficient to simulate $\dot{\alpha}c/U_\infty$ at the static stall angle α_s in order to simulate the dynamic $c_{l_{max}}$. The difference is, of course, that in the case of dynamic airfoil stall (Fig. 18), the near-past time histories $\alpha(t)$ and $\dot{\alpha}(t)$ are very similar, whereas the near-past time histories $\phi(t)$ and $\dot{\phi}(t)$ can be very different in the present case of the rolling delta wing, as was discussed earlier in connection with Figs. 11 and 13. Thus, the release $\phi(0) = -66$ deg corresponds to the case for $\omega t = 126$ deg in Fig. 13. That is, the near past $\dot{\phi}(t)$ is almost invariant. In contrast, the release $\phi(0) = 57$ deg corresponds to $\omega t = 234$ deg in Fig. 13, in which case the near past $\dot{\phi}(t)$ is anything but invariant.

In Fig. 19 the difference in effective roll-rate-induced cambers, including the effects of time lag, is illustrated by the inset sketches. The effective roll angle and roll rate determining the delta wing characteristics at time t are those generated at time $t - \Delta t$. Figure 19 shows that for the $\phi(0) = -66$-deg release the effective roll rate at $t - \Delta t$ is essentially the same as the one at time t, and the effective roll angle is more negative (to the left of $\phi = -5$ deg), resulting in the vortex geometry illustrated in the sketch. That is, the vortex burst has left the leeside wing half and has moved close to the apex on the windward side. Thus, the dynamic effect is to generate a rolling-moment increment $\Delta C_l < 0$. Note that the effect of the roll-rate-induced camber on the unburst vortex contributes also to this negative rolling-moment increment.[21] In contrast, in the case of the $\phi(0) = 57$-deg release, the effective roll rate $\dot{\phi}(t - \Delta t)$ is of the opposite sign to the instantaneous roll rate at time t. The effective roll angle $\phi(t - \Delta t)$ is essentially the same as the instantaneous angle $\phi(t)$.

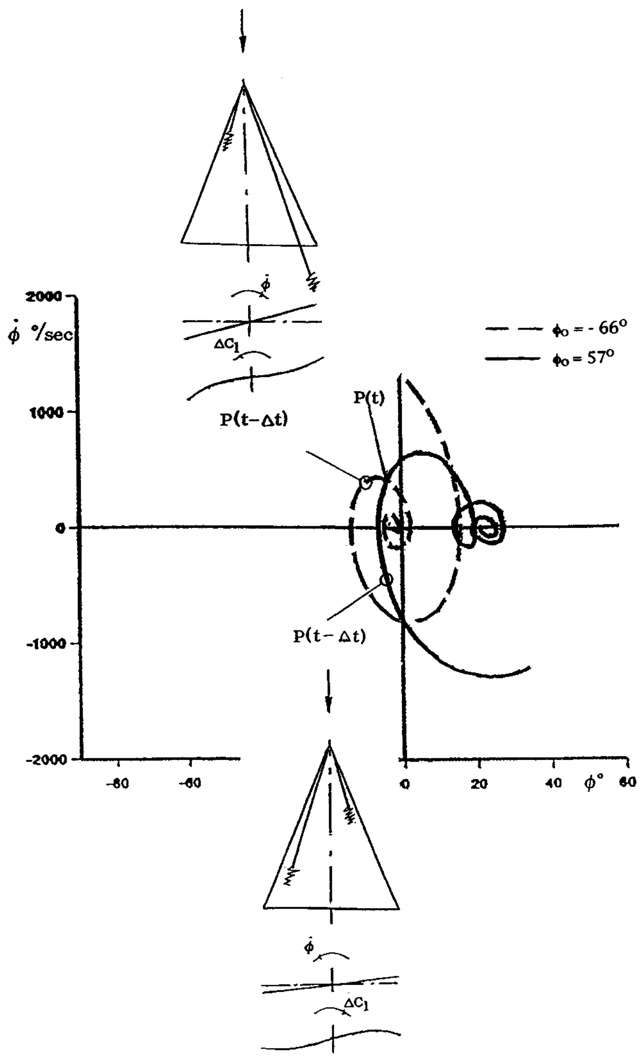

Fig. 19 Flow physics behind phase plane characteristics of free-to-roll motions of a 65-deg delta wing.

The result is that the vortex breakdown moves upstream on the leeward wing half rather than downstream as in the case of the $\phi(0) = -66$-deg release, and moves downstream on the windward wing half. Thus, the dynamic effect is to generate a rolling moment increment $\Delta C_l > 0$. With the help of the flow physics just described one can understand why the $\phi(0) = -66$-deg release converges to the $\phi \approx 0$ trim point, whereas the $\phi(0) = 57$-deg release is "pushed away" from that trim point.

Conclusions

An analysis of the flow physics of the critical states of a 65-deg delta wing rolling at 30-deg inclination of the roll axis provides insight into the combined dynamic effects of roll-rate-induced camber and convective flow time lag. It is clear, however, that extensive further theoretical and experimental research is needed before our understanding will be sufficient for confident prediction of the high-alpha vehicle dynamics.

Acknowledgments

The author is indebted to M. Tobak for his thorough review and to the Technical Editor M. Beyers for his efforts that went well beyond the call of duty.

References

[1]Hanff, E. S., and Jenkins, S. B., "Large-Amplitude High-Rate Roll Experiments on a Delta and Double Delta Wing," AIAA Paper

90-0224, Jan. 1990.

[2]Hanff, E. S., and Ericsson, L. E., "Multiple Roll Attractors of a Delta Wing at High Incidence," AGARD-CP-494, July 1991 (Paper 31).

[3]Jenkins, J. E., Myatt, J. H., and Hanff, E. S., "Body-Axis Rolling Motion Critical States of a 65-Degree Delta Wing," AIAA Paper 93-0621, Jan. 1993.

[4]Ericsson, L. E., and Hanff, E. S., "Unique High-Alpha Roll Dynamics of a Sharp-Edged 65-Deg Delta Wing," *Journal of Aircraft*, Vol. 31, No. 3, 1994, pp. 520–525.

[5]Ericsson, L. E., and Hanff, E. S., "Further Analysis of High-Rate Rolling Experiments of a 65 Deg Delta Wing," *Journal of Aircraft*, Vol. 31, No. 6, 1994, pp. 1350–1357.

[6]Hanff, E. S., and Huang, X. Z., "Roll-Induced Cross-Loads on a Delta Wing at High Incidence," AIAA Paper 91-3223, Sept. 1991.

[7]Wentz, W. H., and Kohlman, D. L., "Vortex Breakdown on Slender Sharp-Edged Wings," *Journal of Aircraft*, Vol. 8, No. 3, 1971, pp. 156–161.

[8]Ericsson, L. E., and King, H. H. C., "Effect of Leading-Edge Cross-Sectional Geometry on Slender Wing Unsteady Aerodynamics," *Journal of Aircraft*, Vol. 30, No. 5, 1993, pp. 793–795.

[9]Lowson, M. V., and Rily, A. J., "Vortex Breakdown Control by Delta Wing Geometry," AIAA Paper 94-3487, Aug. 1994.

[10]Delery, J. M., "Aspects of Vortex Breakdown," *Progress in Aerospace Sciences*, Vol. 30, 1994, pp. 1–59.

[11]Ericsson, L. E., "Aeroelastic Instability Caused by Slender Payloads," *Journal of Spacecraft and Rockets*, Vol. 4, No. 1, 1967, pp. 65–73.

[12]Robertson, J. E., "Unsteady Pressure Phenomena for Basic Missile Shapes at Transonic Speeds," AIAA Paper 64-3, Jan. 1963.

[13]Robertson, J. E., and Chevalier, H. L., "Characteristics of Steady State Pressures on the Cylindrical Portion of Cone-Cylinder Bodies at Transonic Speeds," Arnold Engineering Development Center, TDR-63-104, Aug. 1963.

[14]Chevalier, H. L., and Robertson, J. E., "Pressure Fluctuations Resulting from Alternating Flow Separation and Attachment at Transonic Speeds," Arnold Engineering Development Center, TDR-63-204, Nov. 1963.

[15]Lowson, M. V., "Some Experiments with Vortex Breakdown," *Journal of the Royal Aeronautical Society*, Vol. 68, May 1964, pp. 343–346.

[16]Bergmann, B., Hummel, D., and Oelker, H.-Chr., "Vortex Formation over a Close-Coupled Canard-Wing-Body Configuration in Unsymmetrical Flow," AGARD-CP-494, July 1991 (Paper 14).

[17]Ericsson, L. E., and Reding, J. P., "Fluid Mechanics of Dynamic Stall, Part I, Unsteady Flow Concepts," *Journal of Fluids and Structures*, Vol. 2, No. 1, 1988, pp. 1–33.

[18]Huang, X. Z., and Hanff, E. S., "Prediction of Leading-Edge Vortex Breakdown on a Delta Wing Oscillating in Roll," AIAA Paper 92-2677, June 1992.

[19]Beyers, M. E., and Ericsson, L. E., "Ground Facility Interference on Aircraft Configurations with Separated Flow," *Journal of Aircraft*, Vol. 30, No. 5, 1993, pp. 682–688.

[20]McCroskey, W. J., McAlister, K. W., Carr, L. W., Pucci, S. L., Lambert, O., and Indegrand, R. F., "Dynamic Stall on Advanced Airfoil Sections," *Journal of the American Helicopter Society*, Vol. 26, No. 3, 1981, pp. 40–50.

[21]Ericsson, L. E., and King, H. H. C., "Rapid Prediction of High-Alpha Unsteady Aerodynamics of Slender-Wing Aircraft," *Journal of Aircraft*, Vol. 29, No. 1, 1992, pp. 85–92.